Enhanced Critical Field of Superconductivity at an Oxide Interface

Athby H. Al-Tawhid,[‡] Samuel J. Poage,[‡] Salva Salmani-Rezaie, Antonio Gonzalez, Shalinee Chikara, David A. Muller, Divine P. Kumah, Maria N. Gastiasoro, José Lorenzana, and Kaveh Ahadi*
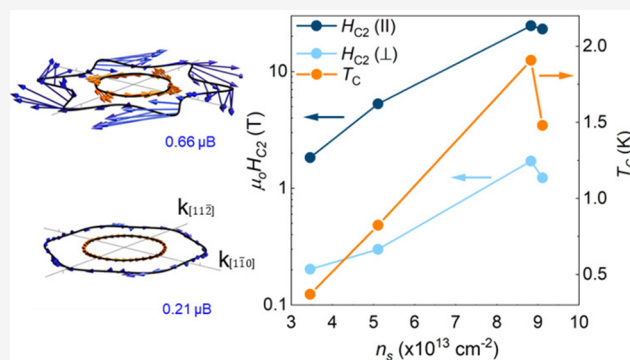
ACCESS | Metrics & More | Article Recommendations | Supporting Information

ABSTRACT: The nature of superconductivity and its interplay with strong spin−orbit coupling at the $KTaO_3(111)$ interfaces remain a subject of debate. To address this problem, we grew epitaxial $LaMnO_3/KTaO_3(111)$ heterostructures. We show that superconductivity is robust against the in-plane magnetic field, with the critical field of superconductivity reaching ∼25 T in optimally doped heterostructures. The superconducting order parameter is highly sensitive to the carrier density. We argue that spin−orbit coupling drives the formation of anomalous quasiparticles with vanishing magnetic moment, providing significant condensate immunity against magnetic fields beyond the Pauli paramagnetic limit. These results offer design opportunities for superconductors with extreme resilience against the applied magnetic fields.

KEYWORDS: *Two-dimensional superconductivity, upper critical field, spin−orbit coupling, Rashba coupling*

Spin−orbit coupling (SOC) in two-dimensional (2D) superconductors gives rise to robust superconductivity against the applied magnetic fields.[1,2] For example, spin−orbit-induced Zeeman spin splitting competes with the in-plane magnetic field in Ising superconductors, stabilizing a highly resilient superconductivity.[3−6] Furthermore, Rashba SOC, creating an in-plane helical spin texture, enhances the superconducting critical field beyond the Pauli paramagnetic limit (H_P).[7] Rashba SOC enhancement of the critical field, however, is limited to $\sqrt{2}\,H_P$.

An important effect of SOC is the generation of states with entangled spin and orbital degrees of freedom, which may lead to single-particle states with vanishing magnetic moments. While the ordering of such "nonmagnetic" electrons in Mott insulators has been studied,[8] itinerant states and the consequences for superconductivity remain unexplored.

$KTaO_3$ is an incipient ferroelectric which remains cubic down to low temperature.[9,10] 2D superconductivity was recently discovered in (111) interfaces.[11] Figure 1a shows the schematic crystal structure of the $KTaO_3(111)$ surface. Itinerant electrons occupy the tantalum 5d-derived t_{2g} states in electron-doped samples.[12,13]

From a magnetic point of view, quasi-particles in $KTaO_3$ can be expected to be highly anomalous. Analogous to photons, which can carry polarization and angular momentum,[14] electronic quasiparticles in $KTaO_3$ carry not only spin $\hat{\mathbf{s}}$ but also orbital angular momentum, $\hat{\mathbf{l}}$. This is due to the strong SOC in the constituent 5d t_{2g} orbitals of Ta. Both $\hat{\mathbf{l}}$ and $\hat{\mathbf{s}}$ contribute to the quasi-particle magnetic moment $\hat{\mathbf{m}} = -\mu_B(\hat{\mathbf{l}} + 2\hat{\mathbf{s}})$. Furthermore, t_{2g} states can be mapped[15,16] into p states
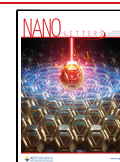
with a fictitious inverted orbital angular momentum $\hat{\mathbf{l}}_p = -\hat{\mathbf{l}}$ (partially quenched from $l = 2$ to $l_p = 1$) and an *effective* total angular momentum $\hat{\mathbf{j}} = (\hat{\mathbf{l}}_p + \hat{\mathbf{s}})$. Figure 1b illustrates the lowest-energy bands of a simplified electronic model of the $KTaO_3(111)$ surface. To a good approximation, the states near Γ have an effective angular momentum $j = 3/2$ in which $\hat{\mathbf{l}}_p$ and $\hat{\mathbf{s}}$ are parallel, implying a magnetic moment $\hat{\mathbf{m}} = -\mu_B(-\hat{\mathbf{l}}_p + 2\hat{\mathbf{s}}) \approx 0$. Figure 1c shows the texture of the magnetic moment $\hat{\mathbf{m}}$ for Fermi surface quasiparticles, illustrating its strong reduction even when the mixing between states with different j is allowed. This remarkable property suggests a small coupling of quasiparticles with an in-plane magnetic field and therefore a strong resilience of superconductivity.
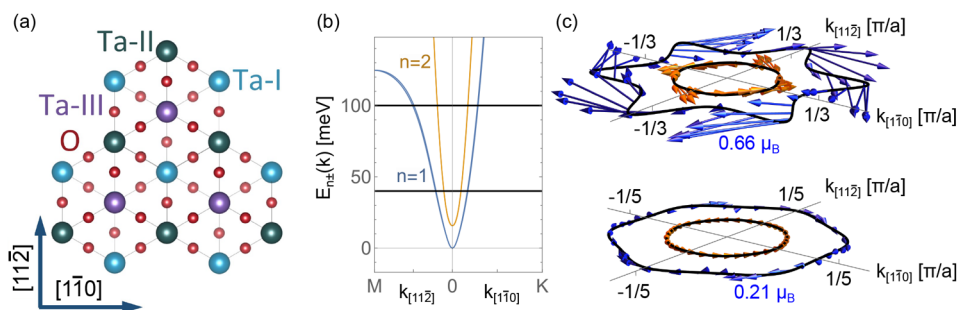
Here we report on the emergence of 2D superconductivity with enhanced critical field and carrier density dependence in molecular beam epitaxy (MBE)-grown $KTaO_3(111)$ epitaxial interfaces. The in-plane critical field (H_{c2}) exceeds the Pauli limit and reaches ∼25 T in optimally doped films. H_{c2} is highly sensitive to the carrier density and magnetic field orientation. To understand the resilience of superconductivity, we computed the critical field in a two-layer model of a $KTaO_3(111)$ interface.
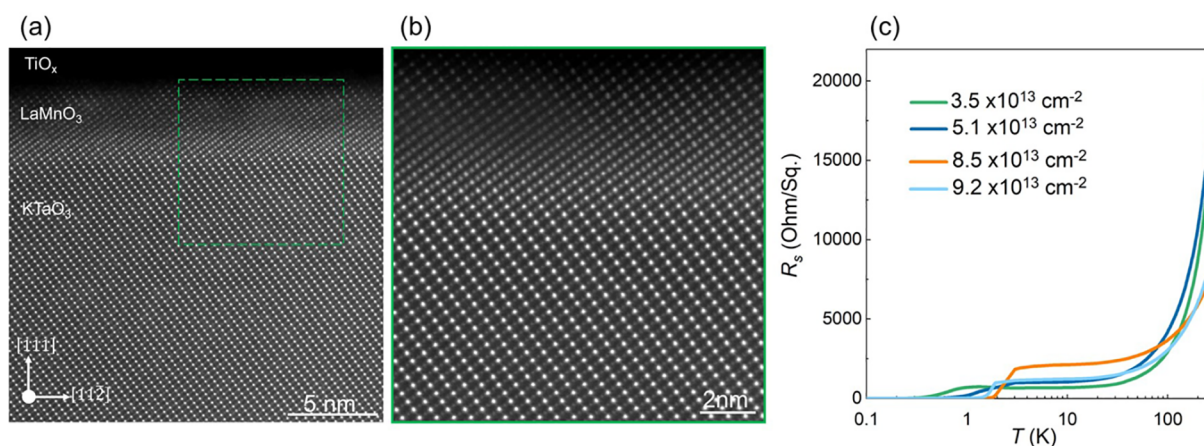
Figure 1. Electronic structure and magnetic moment texture in a KTaO₃(111) 2D electron system. (a) Lattice structure of $KTaO_3(111)$ formed by tantalum and oxygen atoms. (b) Electronic low-energy band structure of $KTaO_3(111)$ in a two-layer model with spin−orbit-coupled t_{2g} orbitals, of mainly $j = 3/2$ character. The two Kramers doublets at the zone center, split by a trigonal crystal field, are further split into opposite-helicity nondegenerate bands at finite k by a small Rashba term (hardly visible in the plot). (c) Fermi surface and magnetic moment texture for chemical potentials $\mu = 40$ meV (bottom) and $\mu = 100$ meV (top) specified by the black lines in (b). For clarity, only the moment of the outer-helicity Rashba band $E_{n-}(k_F)$ is shown for each band: $n = 1$ (blue arrows) and $n = 2$ (orange arrows).
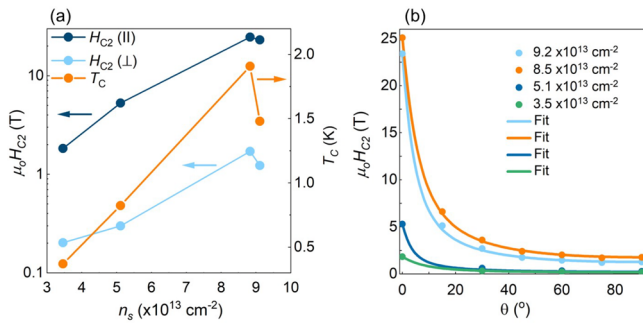

Figure 2. Two-dimensional electron system at the epitaxial LaMnO₃/KTaO₃(111) interfaces. (a) Cross-section HAADF-STEM images of $LaMnO_3$ film grown on a $KTaO_3$ substrate. (b) Higher-magnification HAADF-STEM image of the $LaMnO_3/KTaO_3$ interface. (c) Sheet resistance with temperature (0.1−300 K), suggesting metallic behavior ($dR/dT > 0$) followed by an abrupt superconducting transition.

Epitaxial $LaMnO_3/KTaO_3(111)$ heterostructures were grown by oxide MBE with various 2D electron densities. Figure S1 shows the reflection high-energy electron diffraction (RHEED) streaks, suggesting the 2D growth of $LaMnO_3$. High-angle annular dark-field scanning transmission electron microscopy (HAADF-STEM) was used to investigate the grown heterostructures. Figure 2a shows a HAADF-STEM image of $LaMnO_3$ grown on a $KTaO_3(111)$ substrate. The HAADF-STEM image confirms the epitaxial growth of $LaMnO_3$ on $KTaO_3(111)$. The zoomed-in region shows a continuous bright contrast at the interface which could be due to the steps at the (111) interface.[17] Figure S2 shows the energy-dispersive X-ray spectroscopy (EDX) elemental map across the interface. Figure S3 exhibits the Hall carrier mobility, measured for samples with different carrier densities ($n_s = 3.5 \times 10^{13}$, 5.1×10^{13}, 8.8×10^{13}, and 9.2×10^{13} cm⁻²). The measured 2D carrier densities fall in the range where a superconducting transition is expected.[18] The carrier mobility at liquid helium temperature reaches its maximum, ~300 cm² V⁻¹ s⁻¹ for $n_s = 3.5 \times 10^{13}$ cm⁻², in line with high-quality $KTaO_3(111)$ 2D electron systems.[11] The carrier mobility is systematically suppressed with increasing carrier density.[19,20]

Figure 2c shows the resistance with temperature (300−0.1 K), measured along the $[11\bar{2}]$ direction. All films exhibit metallic behavior ($dR/dT > 0$) followed by an abrupt superconducting transition. Similar heterostructures, grown on a sapphire substrate instead of $KTaO_3$, show insulating behavior, suggesting the transport occurs at the $KTaO_3$ side of the interface. The critical temperature of superconductivity (T_c, defined at $0.1R_n$) is 0.37, 0.82, 1.91, and 1.48 K for $n_s = 3.5 \times 10^{13}$, 5.1×10^{13}, 8.5×10^{13}, and 9.2×10^{13} cm⁻², respectively. These transition temperatures are comparable to those found at $EuO/KTaO_3(111)$ and $LaAlO_3/KTaO_3(111)$ interfaces.[11,21] We estimate the BCS superconducting gap ($\Delta \approx 1.76k_BT_c$) to be 60, 120, 290, and 220 μeV for $n_s = 3.5 \times 10^{13}$, 5.1×10^{13}, 8.5×10^{13}, and 9.2×10^{13} cm⁻², respectively

We further study the superconducting transition by measuring the longitudinal transport with a magnetic field. Figure S4 shows the longitudinal magnetoresistance at different angles between the current and the magnetic field. We find that the in-plane critical fields (H_{c2} defined at $0.9R_n$) are 23.1, 24.7, 5.31, and 1.83 T for $n_s = 9.2 \times 10^{13}$, 8.5×10^{13}, 5.1×10^{13}, and 3.5×10^{13} cm⁻², respectively. Figure 3a compares the critical temperatures and critical fields in hheterostructures with various carrier densities. The critical temperature increases somewhat linearly with carrier density, while the critical field is much more sensitive to the density of charge carriers. Additionally, there is a significant asymmetry between out-of-plane and in-plane H_{c2} results, an effect commonly observed in 2D superconductors.[1] This asymmetry,

Figure 3. Enhanced in-plane H_{c2} at the epitaxial LaMnO$_3$/ KTaO$_3$(111) interfaces. (a) Superconducting transition with carrier density. T_c, $H_{c2,\parallel}$, and $H_{c2,\perp}$ reach their maxima in KTaO$_3$(111) 2D electron system with 8.5×10^{13} cm^{-2} carrier density. The critical temperature increases somewhat linearly with carrier density, while the critical field is much more sensitive to the density of charge carriers. (b) H_{c2} (defined at $0.9R_n$) at various angles between the current and magnetic field measured at the base temperature. Equation 1 describes the results, suggesting 2D superconductivity.

however, varies with carrier density and is illustrated in Figure S5. We also note that the in-plane critical fields exceed the Pauli limit, which we estimate to be $H_P \approx \frac{\Delta}{\sqrt{2}\mu_B}$, assuming a g factor of 2 and weakly coupled superconductivity. Table 1 shows that $H_{c2,\parallel}/H_P$ grows with increasing carrier density.

Figure 3b shows that H_{c2} (defined at $0.9R_n$) follows eq 1, first derived by Tinkham for two-dimensional superconductors:[22]

$$\left| \frac{H_{c2}(\theta) \sin\theta}{H_{c2,\perp}} \right| + \left(\frac{H_{c2}(\theta) \cos\theta}{H_{c2,\parallel}} \right)^2 = 1 \quad (1)$$

Figure S6 shows that the H_{c2} defined at various R_n fractions also follow a similar trend. Figure S7 demonstrates the in-plane and out-of-plane critical fields with temperature, illustrating a monotonic increase of H_{c2} as we cool the sample.

Table 1. Values of T_c (defined at $0.1R_n$), $H_{c2,\parallel}$ and $H_{c2,\perp}$ (defined at $0.9R_n$), Δ ($\approx 1.76k_BT_c$), $H_{c2,\parallel}/H_{c2,\perp}$, and $H_{c2,\parallel}/H_P$ ($H_P \approx \frac{\Delta}{\sqrt{2}\mu_B}$) of KTaO$_3$(111) 2D Electron Systems with Various Carrier Densities (Measured at the Base Temperature)

n_s (cm^{-2})	T_c (K)	$H_{c2,\parallel}$ (T)	$H_{c2,\perp}$ (T)	Δ (μeV)	$H_{c2,\parallel}/H_{c2,\perp}$	$H_{c2,\parallel}/H_P$
3.5×10^{13}	0.37	1.83	0.175	60	10.5	2.7
5.1×10^{13}	0.82	5.31	0.28	120	19.0	3.5
8.5×10^{13}	1.91	24.7	1.71	290	14.4	7.0
9.2×10^{13}	1.48	23.1	1.23	220	18.8	8.4

Table 1 summarizes the measured results in KTaO$_3$(111) interfaces with various carrier densities. The resilience of the superconducting state against in-plane magnetic field and violation of the Pauli limit could be explained by the emergence of the Fulde−Ferrell−Larkin−Ovchinnikov (FFLO) state.[23] In the presence of finite Rashba-type SOC, the FFLO state may arise. The FFLO state, however, emerges in the clean regime ($\Delta\tau_{tr}/\hbar \gg 1$). From the Hall mobility, we estimate the transport relaxation time (see the Supporting Information) as $\tau_{tr} = 3.7 \times 10^{-14}$ s, yielding $\Delta\tau_{tr}/\hbar = 0.003$, for $n_s = 3.5 \times 10^{13}$, deep in the dirty regime. The samples with

higher carrier densities demonstrate an even smaller ratio. The emergence of triplet Cooper pairs could also explain the enhanced critical field, as the Pauli limit does not apply to p-wave superconductors.[24−27] Signatures of mixed-parity superconductivity, however, have not been realized at KTaO$_3$(111) interfaces.[28]

Rashba-type spin splitting was reported at the KTaO$_3$(111) surface.[29] A Rashba SOC acting on spin-1/2 quasiparticles which carry no orbital angular momentum is expected to enhance the Pauli limit by a factor of $\sqrt{2}$.[7] Here, $H_{c2,\parallel}/H_P$ is equal to 2.7 for $n_s = 3.5 \times 10^{13}$ cm^{-2} and increases with carrier density to 8.4 for $n_s = 9.2 \times 10^{13}$ cm^{-2}, much beyond the prediction of a simple Rashba model.

To understand the resilience of the superconductivity against the in-plane magnetic field, we examine the nature of the electronic quasiparticles at the KTaO$_3$(111) surface. The charge accumulation at the KTaO$_3$/LaMnO$_3$ interface creates a negative band-bending potential that can quantize the Ta t_{2g} conduction bands into distinct sub-bands. A (111) bilayer model with three 5d t_{2g} Wannier orbitals per Ta site (yz, zy, xy) and two layers forming a buckled honeycomb plane[30,31] captures many of the key features of the band structure measured by ARPES.[29] This minimal model includes an interlayer nearest-neighbor hopping between Ta-I and Ta-II atoms in Figure 1a, a small trigonal crystal field, the strong local atomic SOC for the 5d t_{2g} orbitals, and a Rashba term due to broken inversion symmetry at the interface (see the Supporting Information for details of the Hamiltonian). The SOC term is diagonalized by states with Wannier orbital angular momentum $l = 1$, yielding at the zone center a low-energy quartet with $j = 3/2$ and a $j = 1/2$ doublet over 400 meV higher in energy.

We can define a Landé g factor for the t_{2g}-derived spin−orbit-coupled states as $\hat{\mathbf{m}} = -\mu_B g_L \hat{\mathbf{j}}$. A textbook computation[32] yields $g_L = 0$ (-2) for the $j = 3/2$ ($1/2$) states, implying zero (finite) magnetic susceptibility. The trigonal crystal field further splits the $j = 3/2$ quartet at the zone center into two Kramers doublets and introduces mixing between the $j = 3/2$ and $j = 1/2$ sectors. Additional mixing of these sectors is also provided by the kinetic energy at finite momenta. This leads to a small but finite magnetic susceptibility of the $j = 3/2$ low-energy bands, certainly much smaller than the Pauli spin susceptibility of free spin-1/2 electrons, as shown below.

The bands emanating from the two Kramers doublets of mainly $j = 3/2$ character are shown in Figure 1b along Γ−M and Γ−K ($n = 1$, blue, and $n = 2$, orange) and will be our main focus. At finite momenta, their double degeneracy is split into opposite-helicity branches $E_{n\pm}(\hat{\mathbf{k}})$ by the inversion-symmetry-breaking Rashba term.

Figure 1c shows the sixfold-symmetric Fermi surface (FS) for the low and high chemical potential (μ) cases specified in Figure 1b. Close to the zone center, both bands show a weakly hexagonal FS (Figure 1c, bottom), and band $n = 1$ develops a star-shaped FS as μ is increased (Figure 1c, top). The magnetic moment texture $\langle\hat{\mathbf{m}}(\mathbf{k})\rangle$, illustrated in the same figure (only for one of the Rashba-split bands, $E_{n-}(k_F)$), is far from the uniform magnetic moment $m_0 = \mu_B$ of free spin-1/2 electrons, which can exhibit a Landau-type orbital angular momentum for perpendicular magnetic fields but do not have a Wannier orbital angular momentum.

As expected for a small g_L, the modulus $m(\mathbf{k})$ of the low-energy spin−orbit-coupled t_{2g} bands is substantially anisotropic, and more importantly, it is significantly smaller than 1

μ_B, the reduction being greater near the zone center. This is clear in Figure 1c, in particular for the portions of the star-shaped Fermi surface closer to the origin and the inner Fermi surface in the upper panel and for both Fermi surfaces in the case of a reduced chemical potential in the lower panel. This strong renormalization of the magnetic moment will have important consequences for the coupling with an in-plane magnetic field, substantially modifying the conventional Pauli paramagnetic response.

Assuming that superconductivity is quenched by Pauli paramagnetic pair breaking, the critical field $H_{c2,\parallel}$ of a system can be estimated by identifying the point where the normal-state and superconducting free energy densities are level: $f_N(H) = f_{SC}(H)$. This condition gives $H_{c2,\parallel} \sim H_P\sqrt{\chi_P/(\chi_N - \chi_{SC})}$, where $H_P = \Delta_0/\sqrt{2}$ is the Pauli field, $\chi_P = \mu_B^2 2N_F$ is the Pauli spin susceptibility of noninteracting electrons with density of states per spin at the Fermi level N_F, and $\chi_{N(SC)}$ is the normal-state (superconducting) magnetic susceptibility. The critical field $H_{c2,\parallel}$ will then exceed H_P when $\chi_{SC} > 0$[7,33] (which happens for a mixed-parity superconducting state) or when the normal-state magnetic susceptibility is reduced ($\chi_N < \chi_P$).[34,35] Since inversion symmetry is broken in the $KTaO_3(111)$ interface, a mixed-parity superconducting state with spin-singlet and spin-triplet components is allowed. However, very little is known in this system about the triplet component of the SC state that would imply a nonzero $\chi_{SC} > 0$. Gor'kov and Rashba[7] estimated a factor of $\sqrt{2}$ enhancement from the mixed SC state in 2D Rashba-split systems, which is much smaller than the enhancement of up to $8.4H_P$ found in this work. We will therefore study and estimate the expected enhancement that arises from $\chi_N < \chi_P$ (which can then be taken as a lower bound of enhancement) and take $\chi_{SC} = 0$.

We compute the normal-state in-plane magnetic susceptibility of band n for a field along the $x \equiv [1\bar{1}0]$ direction as
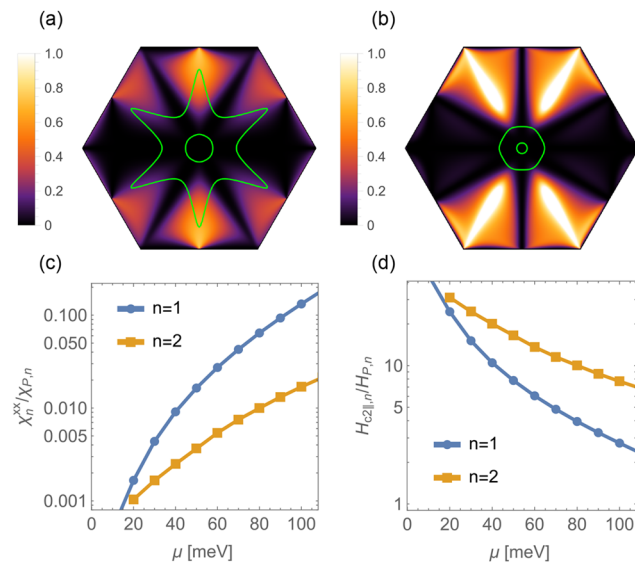
$$\chi_n^{xx} = \mu_B^2 N_F \sum_{\eta=\pm} \gamma_{n\eta,F}^x \tag{2}$$

where $\eta = \pm$ is the helicity index of band $n = 1,2$ (split by the Rashba term), and $\gamma_{n\eta,F}^x$ is the Fermi surface average of the matrix element squared (see the Supporting Information for details),

$$\gamma_{n\eta}^x(\mathbf{k}) = |\langle n\eta\mathbf{k}|(-\hat{l}_p^x + 2\hat{s}^x)|n\eta\mathbf{k}\rangle|^2 \tag{3}$$

which encodes the information of the electronic spin and orbital angular momentum structure. In the case of non-interacting electrons, i.e., without SOC or Rashba, $\gamma_{n\pm}^{xx}(\mathbf{k}) = 1$, and the Pauli susceptibility is recovered: $\chi_n^{xx} = \chi_{P,n} = 2\mu_B^2 N_{F,n}$. Figure 4a,b shows the matrix element $\gamma_{n-}^x(\mathbf{k})$ in the Brillouin zone for both $j = 3/2$-derived low-energy bands in $KTaO_3$, illustrating its strong reduction from unity near the zone center and along particular directions. This reduction in $\gamma_{n\eta}^x(\mathbf{k})$ and hence in $\gamma_{n\eta,F}^x$ implies a reduced magnetic susceptibility (much smaller than the Pauli susceptibility, i.e., $\chi_n^{xx} < \chi_{P,n}$) and hence a strong enhancement of the critical field. Both the SOC and Rashba splitting contribute to this result, as SOC is responsible for the strong reduction of the Landé g factor and Rashba suppresses opposite-chirality mixing, which otherwise would enhance the normal-state susceptibility.

Figure 4c shows the band resolved magnetic susceptibility (eq 2) normalized to the the Pauli susceptibility $\chi_{P,n}$. It is indeed much smaller than unity for small chemical potential

Figure 4. Spin−orbit coupling and Rashba enhancement of $H_{c2,\parallel}$. (a, b) Matrix elements $\gamma_{n-}^x(\mathbf{k})$ from eq 3 for bands (a) $n = 1$ and (b) $n = 2$. The green contours show the Rashba band $E_{n-}(k_F)$ Fermi surface at $\mu = 40$ meV (inner contour) and $\mu = 100$ meV (outer contour). (c) Spin susceptibility χ_n^{xx} of the bands (eq 2) normalized to the Pauli susceptibility $\chi_{P,n}$ as a function of chemical potential. (d) Corresponding $H_{c2,\parallel}$ in units of the band Pauli-limit critical field with chemical potential.

and grows as the Fermi surface expands and departs from the zone center. Figure 4d shows the critical field for each band separately in units of its own Pauli limit field. This very simplified model of the (111) surface explains the large values observed in the experiment for $H_{c2,\parallel}$ regardless of which band has the dominant superconducting order parameter and yields even higher values at low doping.

A notable drawback is that the computation predicts the ratio $H_{c2,\parallel}/H_P$ to decrease with doping, while in the experiment it increases. Since the samples are in the dirty limit, we have also considered impurity effects on the critical field.[36,37] As shown in the Supporting Information, a small contribution of spin−orbit impurity scattering ($\tau_{SO} \gg \tau_{tr}$) can explain the trend of $H_{c2,\parallel}$ with doping. Furthermore, more realistic computations should have more sub-bands over 100 meV higher in energy, as observed by ARPES and attributed to quantum confinement of electrons near the surface.[28,29] These sub-bands have smaller trigonal crystal field splittings,[29] which in our computations would be reflected in purer $j = 3/2$ states with smaller g_L. The population of these sub-bands as doping increases may also reconcile the chemical potential dependence of $H_{c2,\parallel}$ with the experiment. A quantitative computation of this effect requires a multiband theory of superconductivity in $KTaO_3$ that is not available at the moment. More realistic modeling should also take into account the mixing with e_g states[16] and the possibility of a Rashba-induced triplet component of the superconducting state,[7] which could lead to a nontrivial dependence on the density.

In summary, our experimental results demonstrate enhanced $H_{c2,\parallel}$ beyond the Pauli limit, which increases with carrier density. In systems with negligible spin−orbit coupling, electrons behave as spin-1/2 particles and therefore carry a 1 μ_B magnetic moment. We argue that the $KTaO_3(111)$ interface hosts quasiparticles that carry a very small magnetic moment.

This makes superconductivity largely immune to the Pauli paramagnetism and explains the anomalous enhancement of the in-plane critical field. One can still assign a pseudo-spin-1/2 quantum number to the quasiparticles, so Cooper pairing proceeds as usual among time-reversal partners. These results offer opportunities to enhance H_{c2} by tuning the electronic structure and spin texture in crystalline 2D superconductors with strong spin−orbit coupling.

■ MATERIALS AND METHODS

Heterostructures were grown by oxide MBE with a base pressure of 2×10^{-10} Torr. The carrier density was controlled with growth parameters as described elsewhere.[28,38,39] Ten unit cells of $LaMnO_3$ were grown, followed by TiO_x (1−3 nm), on the $KTaO_3$(111) substrate. The elemental fluxes, emanating from effusion cells, were calibrated using a quartz crystal microbalance (QCM).

The substrate was annealed for 30 min prior to the growth at 600 °C and subsequently heated to 800 °C, and growth was started immediately to avoid potassium loss. The oxygen partial pressure was 3×10^{-6} Torr during $LaMnO_3$ growth. Reflection high-energy electron diffraction (RHEED) showed diffraction streaks, suggesting smooth $LaMnO_3$ films (Figure S1). The samples were cooled to 550 °C immediately after the growth of $LaMnO_3$ to grow a TiO_x amorphous layer (∼3 nm). Disappearance of the RHEED streaks confirmed the amorphous nature of the TiO_x layer. Finally, a 20 nm amorphous lanthanum oxide layer was grown as a capping layer, protecting the 2D electron gas from oxidation. The growth was repeated on a sapphire substrate, which resulted in an insulating behavior (∼1−10 MΩ).

Scanning transmission electron microscopy (STEM) and energy-dispersive X-ray spectroscopy (EDX) were performed to study the films and their interface structures. EDX data were collected using a steradian Dual-X EDX detector with a probe current of 60 pA. Cross-sectional samples were prepared using a Thermo Fisher Scientific Helios G4UX focused ion beam. High-angle annular dark-field (HAADF) images were obtained using a Thermo Fisher Scientific Spectra 300 X-CFEG operating at 200 kV with a convergence angle of 30 mrad and a HAADF detector with an angular range of 60−200 mrad.

The high-temperature (300−3 K) magnetoelectric measurements were carried out in a Quantum Design Physical Property Measurement System (PPMS). Transport measurements were carried out in van der Pauw geometry with square-shaped samples and gold contacts deposited on the sample corners by using a sputtering system. The Hall coefficient was calculated from a linear fit to R_{xy} with magnetic field ($R_H = dR_{xy}/dB$). The Hall carrier density was extracted from $n_{2D} = -1/(eR_H)$, where e is the electron charge.

The subkelvin magnetoelectric measurements were carried out in an Oxford dilution refrigerator with a base temperature of 8 mK (50 mK with the application of high field). The lines were filtered to avoid microwave radiation. The superconductivity measurements were carried out using a lock-in amplifier (SR860) and a current source (CS580) at 1 μA. The critical field was measured by sweeping the magnet (32 T superconducting magnet) at various temperatures and angles at the National High Magnetic Field Laboratory.

■ ASSOCIATED CONTENT

Data Availability Statement

The data that support the findings of this study are available in the article and its Supporting Information. Raw data can be obtained from the corresponding authors upon request.

ⓢ Supporting Information

The Supporting Information is available free of charge at https://pubs.acs.org/doi/10.1021/acs.nanolett.3c01571.

RHEED during and after the growth, STEM-EDX across the interface, Hall carrier mobility, longitudinal magnetoresistance at various angles, $H_{c2,\|}/H_{c2,\perp}$ and $H_{c2,\|}/H_P$ with carrier density, H_{c2} at various angles and temperatures, and $H_{c2,\|}$ calculated using the KLB equation (PDF)

■ AUTHOR INFORMATION

Corresponding Author

Kaveh Ahadi − *Department of Materials Science and Engineering, North Carolina State University, Raleigh, North Carolina 27265, United States; Department of Physics, North Carolina State University, Raleigh, North Carolina 27695, United States;* ⓞ orcid.org/0000-0003-2280-4037; Email: kahadi@ncsu.edu

Authors

Athby H. Al-Tawhid − *Department of Materials Science and Engineering, North Carolina State University, Raleigh, North Carolina 27265, United States*

Samuel J. Poage − *Department of Materials Science and Engineering, North Carolina State University, Raleigh, North Carolina 27265, United States*

Salva Salmani-Rezaie − *School of Applied and Engineering Physics, Cornell University, Ithaca, New York 14853, United States; Kavli Institute at Cornell for Nanoscale Science, Cornell University, Ithaca, New York 14853, United States*

Antonio Gonzalez − *Department of Materials Science and Engineering, North Carolina State University, Raleigh, North Carolina 27265, United States*

Shalinee Chikara − *National High Magnetic Field Laboratory, Tallahassee, Florida 32310, United States*

David A. Muller − *School of Applied and Engineering Physics, Cornell University, Ithaca, New York 14853, United States; Kavli Institute at Cornell for Nanoscale Science, Cornell University, Ithaca, New York 14853, United States*

Divine P. Kumah − *Department of Physics, North Carolina State University, Raleigh, North Carolina 27695, United States*

Maria N. Gastiasoro − *Donostia International Physics Center, 20018 Donostia-San Sebastian, Spain*

José Lorenzana − *ISC−CNR and Department of Physics, Sapienza University of Rome, 00185 Rome, Italy;* ⓞ orcid.org/0000-0001-7426-2570

Complete contact information is available at:
https://pubs.acs.org/10.1021/acs.nanolett.3c01571

Author Contributions

‡A.H.A.-T. and S.J.P. contributed equally to this work.

Notes

The authors declare no competing financial interest.

■ REFERENCES

(1) Saito, Y.; Nojima, T.; Iwasa, Y. Highly crystalline 2D superconductors. *Nat. Rev. Mater.* **2017**, *2*, 16094.

(2) Zhang, D.; Falson, J. Ising pairing in atomically thin superconductors. *Nanotechnology* **2021**, *32*, 502003.

(3) Lu, J.; Zheliuk, O.; Leermakers, I.; Yuan, N. F.; Zeitler, U.; Law, K. T.; Ye, J. Evidence for two-dimensional Ising superconductivity in gated MoS$_2$. *Science* **2015**, *350*, 1353−1357.

(4) Xi, X.; Wang, Z.; Zhao, W.; Park, J.-H.; Law, K. T.; Berger, H.; Forró, L.; Shan, J.; Mak, K. F. Ising pairing in superconducting NbSe$_2$ atomic layers. *Nat. Phys.* **2016**, *12*, 139−143.

(5) Falson, J.; Xu, Y.; Liao, M.; Zang, Y.; Zhu, K.; Wang, C.; Zhang, Z.; Liu, H.; Duan, W.; He, K.; Liu, H.; Smet, J.; Zhang, D.; Xue, Q.-K. Type-II Ising pairing in few-layer stanene. *Science* **2020**, *367*, 1454−1457.

(6) Rhodes, D. A.; Jindal, A.; Yuan, N. F.; Jung, Y.; Antony, A.; Wang, H.; Kim, B.; Chiu, Y.-c.; Taniguchi, T.; Watanabe, K.; Barmak, K.; Balicas, L.; Dean, C.; Qian, X.; Fu, L.; Pasupathy, A.; Hone, J. Enhanced superconductivity in monolayer T_d-MoTe$_2$. *Nano Lett.* **2021**, *21*, 2505.

(7) Gor'kov, L. P.; Rashba, E. I. Superconducting 2D system with lifted spin degeneracy: mixed singlet-triplet state. *Phys. Rev. Lett.* **2001**, *87*, 037004.

(8) Ishikawa, H.; Takayama, T.; Kremer, R. K.; Nuss, J.; Dinnebier, R.; Kitagawa, K.; Ishii, K.; Takagi, H. Ordering of hidden multipoles in spin-orbit entangled 5d^1 Ta chlorides. *Phys. Rev. B* **2019**, *100*, 045142.

(9) Shirane, G.; Nathans, R.; Minkiewicz, V. Temperature Dependence of the Soft Ferroelectric Mode in KTaO$_3$. *Phys. Rev.* **1967**, *157*, 396.

(10) Schwaigert, T.; Salmani-Rezaie, S.; Barone, M. R.; Paik, H.; Ray, E.; Williams, M. D.; Muller, D. A.; Schlom, D. G.; Ahadi, K. Molecular beam epitaxy of KTaO$_3$. *J. Vac. Sc. Technol. A* **2023**, *41*, 022703.

(11) Liu, C.; Yan, X.; Jin, D.; Ma, Y.; Hsiao, H.-W.; Lin, Y.; Bretz-Sullivan, T. M.; Zhou, X.; Pearson, J.; Fisher, B.; Jiang, S.; Han, W.; Zuo, J.-M.; Wen, J.; Fong, D.; Sun, J.; Zhou, H.; Bhattacharya, A. Two-dimensional superconductivity and anisotropic transport at KTaO$_3$ (111) interfaces. *Science* **2021**, *371*, 716.

(12) Himmetoglu, B.; Janotti, A. Transport properties of KTaO$_3$ from first-principles. *J. Phys.: Condens. Matter* **2016**, *28*, 065502.

(13) Al-Tawhid, A. H.; Kanter, J.; Hatefipour, M.; Irving, D. L.; Kumah, D. P.; Shabani, J.; Ahadi, K. Oxygen Vacancy-Induced Anomalous Hall Effect in a Nominally Non-magnetic Oxide. *J. Electron. Mater.* **2022**, *51*, 7073−7077.

(14) Bliokh, K. Y.; Nori, F. Transverse and longitudinal angular momenta of light. *Phys. Rep.* **2015**, *592*, 1−38.

(15) Sugano, S.; Tanabe, Y.; Kamimura, H. *Pure and Applied Physics*; Academic Press: New York, 1970; Vol. *33*.

(16) Stamokostas, G. L.; Fiete, G. A. Mixing of t$_{2g}$−e$_g$ orbitals in 4d and 5d transition metal oxides. *Phys. Rev. B* **2018**, *97*, 085150. arXiv:1711.02328.

(17) Raghavan, S.; Zhang, J. Y.; Stemmer, S. Two-dimensional electron liquid at the (111) SmTiO$_3$/SrTiO$_3$ interface. *Appl. Phys. Lett.* **2015**, *106*, 132104.

(18) Liu, C.; Zhou, X.; Hong, D.; Fisher, B.; Zheng, H.; Pearson, J.; Jiang, J. S.; Jin, D.; Norman, M. R.; Bhattacharya, A. Tunable superconductivity and its origin at KTaO$_3$ interfaces. *Nat. Commun.* **2023**, *14*, 951.

(19) Ahadi, K.; Stemmer, S. Novel metal-insulator transition at the SmTiO$_3$/SrTiO$_3$ interface. *Phys. Rev. Lett.* **2017**, *118*, 236803.

(20) Ahadi, K.; Kim, H.; Stemmer, S. Spontaneous Hall effects in the electron system at the SmTiO$_3$/EuTiO$_3$ interface. *APL Mater.* **2018**, *6*, 056102.

(21) Chen, Z.; Liu, Y.; Zhang, H.; Liu, Z.; Tian, H.; Sun, Y.; Zhang, M.; Zhou, Y.; Sun, J.; Xie, Y. Electric field control of superconductivity at the LaAlO$_3$/KTaO$_3$ (111) Interface. *Science* **2021**, *372*, 721−724.

(22) Tinkham, M. Effect of fluxoid quantization on transitions of superconducting films. *Phys. Rev.* **1963**, *129*, 2413.

(23) Fulde, P.; Ferrell, R. A. Superconductivity in a strong spin-exchange field. *Phys. Rev.* **1964**, *135*, A550.

(24) Schumann, T.; Galletti, L.; Jeong, H.; Ahadi, K.; Strickland, W. M.; Salmani-Rezaie, S.; Stemmer, S. Possible signatures of mixed-parity superconductivity in doped polar SrTiO$_3$ films. *Phys. Rev. B* **2020**, *101*, 100503.

(25) Ahadi, K.; Galletti, L.; Li, Y.; Salmani-Rezaie, S.; Wu, W.; Stemmer, S. Enhancing superconductivity in SrTiO$_3$ films with strain. *Sci. Adv.* **2019**, *5*, eaaw0120.

(26) Russell, R.; Ratcliff, N.; Ahadi, K.; Dong, L.; Stemmer, S.; Harter, J. W. Ferroelectric enhancement of superconductivity in compressively strained srtio 3 films. *Phys. Rev. Mater.* **2019**, *3*, 091401.

(27) Salmani-Rezaie, S.; Ahadi, K.; Stemmer, S. Polar nanodomains in a ferroelectric superconductor. *Nano Lett.* **2020**, *20*, 6542−6547.

(28) Arnault, E. G.; Al-Tawhid, A. H.; Salmani-Rezaie, S.; Muller, D. A.; Kumah, D. P.; Bahramy, M. S.; Finkelstein, G.; Ahadi, K. Anisotropic superconductivity at KTaO$_3$(111) interfaces. *Sci. Adv.* **2023**, *9*, eadf1414.

(29) Bruno, F. Y.; McKeown Walker, S.; Riccò, S.; De La Torre, A.; Wang, Z.; Tamai, A.; Kim, T. K.; Hoesch, M.; Bahramy, M. S.; Baumberger, F. Band Structure and Spin-Orbital Texture of the (111)-KTaO$_3$ 2D Electron Gas. *Adv. Electron. Mater.* **2019**, *5*, 1800860.

(30) Xiao, D.; Zhu, W.; Ran, Y.; Nagaosa, N.; Okamoto, S. Interface engineering of quantum Hall effects in digital transition metal oxide heterostructures. *Nat. Commun.* **2011**, *2*, 596.

(31) Villar Arribi, P.; Paramekanti, A.; Norman, M. R. Striped electron fluid on (111) KTaO$_3$. *Phys. Rev. B* **2021**, *103*, 035115.

(32) Ashcroft, N. W.; Mermin, N. D. *Solid State Physics*; Holt, Rinehart and Winston: New York, 1976.

(33) Yip, S. K. Two-dimensional superconductivity with strong spin-orbit interaction. *Phys. Rev. B* **2002**, *65*, 144508.

(34) Yip, S.-K. Models of superconducting cu:bi$_2$se$_3$: Single- versus two-band description. *Phys. Rev. B* **2013**, *87*, 104505.

(35) Xie, Y.-M.; Zhou, B. T.; Law, K. T. Spin-Orbit-Parity-Coupled Superconductivity in Topological Monolayer wte$_2$. *Phys. Rev. Lett.* **2020**, *125*, 107001.

(36) Werthamer, N. R.; Helfand, E.; Hohenberg, P. C. Temperature and Purity Dependence of the Superconducting Critical Field, H$_{c2}$. iii. Electron Spin and Spin-Orbit Effects. *Phys. Rev.* **1966**, *147*, 295−302.

(37) Klemm, R. A.; Luther, A.; Beasley, M. R. Theory of the upper critical field in layered superconductors. *Phys. Rev. B* **1975**, *12*, 877−891.

(38) Al-Tawhid, A. H.; Kanter, J.; Hatefipour, M.; Kumah, D. P.; Shabani, J.; Ahadi, K. Superconductivity and Weak Anti-localization at $KTaO_3$ (111) Interfaces. *J. Electron. Mater.* **2022**, *51*, 6305−6309.

(39) Al-Tawhid, A. H.; Kumah, D. P.; Ahadi, K. Two-dimensional electron systems and interfacial coupling in $lacro_3/KTaO_3$ heterostructures. *Appl. Phys. Lett.* **2021**, *118*, 192905.

📖 Recommended by ACS

Ambipolar Superconductivity with Strong Pairing Interaction in Monolayer 1T′-MoTe₂

Fangdong Tang, Jurgen H. Smet, *et al.*

AUGUST 04, 2023
NANO LETTERS   READ ↗

Fourfold Symmetric Superconductivity in Spinel Oxide $LiTi_2O_4$(001) Thin Films

Huanyi Xue, Wei Li, *et al.*

NOVEMBER 04, 2022
ACS NANO   READ ↗

Two-Dimensional Superconductivity at the Titanium Sesquioxide Heterointerface

Lijie Wang, Wei Li, *et al.*

SEPTEMBER 19, 2022
ACS NANO   READ ↗

Unconventional Superconductivity at $LaVO_3/SrTiO_3$ Interfaces

Soumyadip Halder, Goutam Sheet, *et al.*

NOVEMBER 21, 2022
ACS APPLIED ELECTRONIC MATERIALS   READ ↗

Get More Suggestions >